Effect of the Linker and Substituents on the Ionic Conductivity of Borate Single-Ion Polymers for Lithium Batteries

Soline Vauthier[1,2], Stéphane Cotte[2], Laurent Castro[2], Aurélie Guéguen[2], Nerea Casado[1,4], David Mecerreyes[1,4], Gregorio Guzmán-Gonzalez[*1,3]

[1]POLYMAT, University of the Basque Country UPV/EHU, Joxe Mari Korta Center, Avda. Tolosa 7, 20018 Donostia-San Sebastian, Spain.
[2]Toyota Motor Europe Research and Development 1, Advanced Material Research Battery and Fuel Cell, Hoge Wei 33, Zaventem B-1930, Belgium.
[3]Departamento de Química, Universidad Autónoma Metropolitana-Iztapalapa, 09340, México City, México.
[4]IKERBASQUE, Basque Foundation for Science, 48009, Bilbao, Spain.

*Corresponding author: Gregorio Guzmán-Gonzalez, email: greg@xanum.uam.mx

Abstract. Polymer electrolytes with high ionic conductivity are actively searched for their application as solid electrolytes in lithium batteries. Here, we show new borate single lithium-ion conducting polymers with high ionic conductivity and lithium transference number values. For this purpose, eight new methacrylic lithium borate polymers were synthesized and characterized with varying chemical compositions focusing on the linker between the polymer chain and the pendant borate ionic group and its substituents. The polymers with the optimum ethoxy linker and fluorinated pendant groups show a low Tg value and the highest ionic conductivity value of 1.29×10^{-4} S.cm^{-1} at 60 °C. This value is among the highest ionic conductivity reported for a single lithium-ion conducting homopolymer. These polymers show a high lithium transference number (between 0.88 and 0.96) and electrochemical stability close to 4.2 V vs Li$^+$/Li, making them promising candidates for application as solid electrolytes in lithium batteries.
Keywords: Lithium-ion; lithium-ion batteries; polymer electrolytes; ion transport; solid electrolyte.

Resumen. Se buscan activamente electrolitos poliméricos con alta conductividad iónica para su aplicación como electrolitos sólidos en baterías de litio. Aquí, mostramos nuevos polímeros conductores de iones de litio de borato simples con valores muy altos de conductividad iónica y número de transferencia de litio. Para ello, se sintetizaron y caracterizaron ocho nuevos polímeros metacrílicos de borato de litio con composiciones químicas variables centradas en el enlazador entre la cadena polimérica y el grupo iónico borato colgante y sus sustituyentes. Los polímeros con el enlazador etoxi óptimo y los grupos colgantes fluorados muestran un valor Tg bajo y un valor superior de conductividad iónica $1,29 \times 10^{-4}$ Scm^{-1} a 60 °C. Este valor es uno de los más altos de conductividad iónica a 60 °C. Este valor es uno de los valores más altos de conductividad iónica a 60 °C. Este valor es uno de los más altos valores de conductividad iónica registrados para un solo homopolímero conductor de iones de litio. Estos polímeros muestran un elevado número de transferencia de litio (entre 0.88 y 0.96), y una estabilidad electroquímica cercana a 4.2 V vs Li$^+$/Li que los convierten en candidatos prometedores para su aplicación como electrolitos sólidos en baterías de litio.
Palabras clave: Ion-litio; baterías de ion-litio; electrolitos poliméricos; transporte de iones; electrolito sólido.

Special issue: Celebrating 50 years of Chemistry at the Universidad Autónoma Metropolitana. Part 1

Introduction

Solid polymer electrolytes (SPEs) are of interest for developing the next generation of solid-state batteries for applications such as electric vehicles where safety is necessary. The main properties sought for SPEs are high ionic conductivity,[1] good mechanical strength, high lithium transference number, thermal and electrochemical stabilities, and good compatibility with electrodes.[2,3] Polyethers such as PEO are the most popular polymers for SPEs due to their ability to dissolve lithium salts by electrostatic interactions between ether oxygens and lithium ions.[4–6] Nowadays, poly(ethylene oxide) (PEO) is the standard polymer matrix for SPEs, part of commercial solid-state lithium batteries for the transportation sector.[4,7] The optimized PEO SPEs show high ionic conductivity values in the order of 10^{-3} S.cm^{-1} at 70 °C.[8] However, their low lithium transference numbers ($t_{Li^+} < 0.25$) and electrochemical stability window (< 4.2 V vs Li$^+$/Li) limit their applications in lithium metal batteries with high-voltage cathodes.

Single lithium-ion conducting polymer electrolytes (SLICPEs) are a family of SPEs composed of an anionic polyelectrolyte with lithium counter-ion.[9] They show a lithium transference number close to unity ($t_{Li^+} \approx 1$).[3,10,11] Its high interest is due to the limited formation of ionic concentration gradients in the solid electrolyte, which can limit dendritic growth on the lithium anode. However, in most cases, the overall ionic conductivity of SLICPEs is much lower than one of the best PEO SPEs.[12]

Nowadays, the SLIPCEs with the highest ionic conductivity are based on anionic polyelectrolytes having sulphonamides [13] or tetrahedral borates.[14,15] These single-ion conducting homopolymers show ionic conductivity values still lower than 1×10^{-6} S cm^{-1}, e.g. Poly(LiMTFSI), [16,17] and Poly(STFSI)[18,19] with 1×10^{-12} and 7.6×10^{-6} S cm^{-1} at 25 °C, respectively or 6×10^{-6} S.cm^{-1} at 25 °C for lithium polyvinyl alcohol oxalate borate (LiPVAOB).[20] These values of the SLICPEs can be increased by blending with other polymers such as PEO.[21–23] For instance, Olmedo-Martínez et al. [24] measured an ionic conductivity of 2.1×10^{-4} S.cm^{-1} at 70 °C for an optimized mixture of PEO with Poly(LiMTFSI). In another example, Meabe et al. measured an ionic conductivity of 3.2×10^{-5} Scm^{-1} at 25°C with a blend of PEO and LiFSI.[25] Very recently, we reported a new family of single lithium-ion conducting polymer electrolytes based on highly delocalized borate groups.[1] The synthesis and the effect of the nature of the pendant substituents linked to the boron atom on the ionic conductivity were reported, highlighting the highest ionic conductivity reported for a single lithium-ion conducting polymer of 10^{-4} Scm^{-1} at 60 °C.[26]

The main objective of this article is to investigate the effect of the ethoxy linker between the polymer chain and the borate group and its substituents to increase further the ionic conductivity of borate-based single lithium-ion conducting polymers.[27,28] After establishing the optimal ethoxy linker length and based on the previous work investigating the different substituent groups, optimized SLICPEs with varying pendant groups are presented, and their ionic conductivities are discussed. An in-depth study of the influence of the fluorine substituents on the ionic conductivity of SLICPEs is presented, and the relation between the electron density of borate groups and the number of ethoxy groups serving as ionic transport pathways in SLICPEs is discussed. Finally, the lithium transference number and electrochemical stability window for polymer electrolytes were assessed to confirm their potential for lithium battery applications.

Experimental

Materials

All chemicals, including 2-Hydroxyethyl methacrylate (HEMA, 97 %, Aldrich), Poly(ethylene glycol) methacrylate (PEGMA, molecular weight of 360 and 500 g•mol^{-1}, Aldrich), Borane tetrahydrofuran complex solution 1.0 M in THF (BH$_3$, Aldrich), n-Butyl lithium 2.5M solution in hexanes, (nBuLi, ACROS), 2,2′-Azobisisobutyronitrile (AIBN, initiator, 98 %, Aldrich), Trimethyl borate (TMB, ≥98 %, Aldrich), Triethyl borate (TEB, ≥95%, Aldrich), Triisopropyl borate (TiPB, ≥98 %, Aldrich), 1,1,1,3,3,3-Hexafluoro-2-propanol (HFiP, ≥99%, Aldrich), 1,1,1-Trifluoro-2-propanol (TFP, 97 %, Aldrich), were used as received. Triethylene glycol monomethyl ether (TEG, 95%, Aldrich) was distilled at the rotary evaporator at 70 °C and reduced pressure. The methanol (MeOH) and hexane solvents from Scharlab were dried with anhydrous MgSO$_4$ before

Special issue: Celebrating 50 years of Chemistry at the Universidad Autónoma Metropolitana. Part 1

use. BH_3-THF complex and n-Butyl lithium are highly moisture-sensitive reagents, so they must be handled under an inert atmosphere in all steps.

Methods

NMR spectra were recorded for ^{1}H, ^{19}F, and ^{11}B NMR spectroscopy analysis with the Avance III 400 MHz. Fourier transform infrared (FT-IR) spectra were obtained using the Nicolet 6700 FTIR spectrometer over the 4000-400 cm^{-1} range. The thermal properties of the polymers were evaluated by DSC (SDTQ-600 TA instruments) with a heating rate of 10 °C/min^{-1} from -70 to 100 °C under N_2 flow. The glass transition temperatures (Tg) were measured by the onset temperature extrapolated in the second heating scan.

Ionic conductivity values were obtained by EIS measurements using an Autolab 302N potentiostat/galvanostat (Metrohm AG) equipped with a temperature controller (Microcell HC station). The samples were placed between two stainless steel electrodes with a surface area of 0.5 cm^2 and a thickness of 0.1 mm. The measurements were performed every 10 °C between 95 and 25 °C with a frequency range set from 0.1 MHz to 0.1 Hz and 10 mV amplitude. The ionic conductivity values of SLICPEs were calculated following equation (1) based on literature:[29]

$$\sigma = (1/R_b).(d/S) \tag{1}$$

where σ is the ionic conductivity (S cm^{-1}), d is the thickness (cm), S is the area (cm^2) of the stainless-steel electrodes, R_b (Ω) is the bulk resistance extracted from the Nyquist plot obtained by EIS. Each test was repeated at least three times, and the results showed an average with the standard deviation. The activation energy E_a of SLICPEs was calculated according to Arrhenius equation (2) based on literature:[30,31]

$$\sigma = \sigma_0.exp(-E_a/RT) \tag{2}$$

where σ_0 is the pre-exponential factor related to the conductivity at infinite temperature, E_a is the activation energy for ion mobility, R is the universal gas constant (8.314 J mol^{-1} K^{-1}), and T is the absolute temperature.

The lithium-ion transference numbers (t_{Li+}) were evaluated in Li|SLICPE|Li symmetric coin cells employing the direct current (DC) polarization/alternating current (AC) impedance method. A 10 mV (ΔV) potential is applied to polarize the SLICPEs during chronoamperometry. t_{Li+} were calculated following the equation (3) proposed by the Evans-Vincent-Bruce method:[32,33]

$$t_{Li+}=(I_{ss}(\Delta V - I_0 R_0))/(I_0(\Delta V - I_{ss} R_{ss})) \tag{3}$$

where I_{ss} is the steady-state current for the sample polarized, I_0 is the initial value of the current upon polarization, R_{ss} and R_0 does EIS obtain the electrode resistances after and before the polarization, respectively.

The electrochemical stability windows were evaluated with a Li|SLICPE|stainless-steel coin cell, using linear sweep voltammetry (LSV) in a range from 2 to 6 V vs Li$^+$/Li at a scan rate of 0.2 mVs^{-1} at 25 °C.

General procedure of lithium-ion monomer synthesis

A series of lithium borate methacrylic salts was synthesized. Their general chemical structure called *LBBn(OR)$_2$* is represented in Fig. 1(**a**). They are composed of a methacrylic acid group for polymer network formation by the polymerization reaction, an ethoxy chain, where different lengths are investigated (n=1, 7, and 9); a single ion part, with a boron atom as the anionic center ionically bonded to a mobile lithium ion; a butyl function giving rise to the B-C bond; and two pendant groups (-OR), on which different functions are tested (such as moderate and high electron-withdrawing or self-solvation capabilities) for modulation of the electron density of the borate groups.

The seven monomers substituted with aliphatic groups (-R) such as methyl, ethyl, and isopropyl (LBBn$_1$(OMe)$_2$, LBBn$_7$(OMe)$_2$, LBBn$_9$(OMe)$_2$, LBBn$_1$(OEt)$_2$, LBBn$_7$(OEt)$_2$, LBBn$_1$(OiP)$_2$, and LBBn$_7$(OiP)$_2$) were synthesized following the method A as shown in Fig. 1(**a-b**). To synthesize the three monomers, LBBn$_1$(OMe)$_2$, LBBn$_1$(OEt)$_2$, and LBBn$_1$(OiP)$_2$, HEMA (10 mmol, 1.3 g) and dry hexane (30 ml) were charged

561

into a flask of 100 ml. Concerning the three monomers synthesis of LBBn$_7$(OMe)$_2$, LBBn$_7$(OEt)$_2$, and LBBn$_7$(OiP)$_2$, PEGMA with a molecular weight of 360 g.mol^{-1} (10 mmol, 3.6 g) and dry hexane (30 ml) were charged into a flask of 100 ml. Then, for LBBn$_9$(OMe)$_2$ synthesis, PEGMA with a molecular weight of 500 g.mol^{-1} (10 mmol, 5.0 g) and dry hexane (30 ml) were charged into a flask of 100 ml. Then, the solutions were stirred with argon flow and cooled in an acetone-liquid nitrogen bath, ensuring a constant magnetic stirring to avoid solidification of the system. 1 molar equivalent (1 eq.) of Tri-R borates "B(OR)$_3$" was added dropwise according to the desired monomer. TMB (10 mmol, 1.04 ml) for LBBn$_1$(OMe)$_2$, LBBn$_7$(OMe)$_2$, and LBBn$_9$(OMe)$_2$ monomers synthesis. TEB (10 mmol, 1.7 ml) for LBBn$_1$(OEt)$_2$ and LBBn$_7$(OEt)$_2$ monomers synthesis. TiPB (10 mmol, 2.2 ml) for LBBn$_1$(OiP)$_2$ and LBBn$_7$(OiP)$_2$ monomers synthesis. The reaction mixtures were slowly heated to RT and stirred for 2 h. Subsequently, the systems were cooled again in an acetone-liquid nitrogen bath, and 1 eq. of nBuLi 2.5 M in hexane (10 mmol, 4 ml) was added dropwise. The precipitates formed were heated to RT and stirred for another 2 h more before being filtered and washed with cold diethyl ether. The white monomers obtained were placed in vials and dried on a vacuum line at 40 °C for 24h.

The method B shown in Fig. 1**(a)** and Fig. 1**(c)** was followed to synthesize the monomers LBBn$_1$(OF$_6$iP)$_2$, LBBn$_7$(OF$_6$iP)$_2$, LBBn$_7$(OF$_3$iP)$_2$, LBBn$_1$(OGly)$_2$, LBBn$_1$(OGlyOF$_6$iP), and LBBn$_1$(OGlyOF$_3$iP). 30 ml of dry hexane were charged into the 100 ml two-neck flask with HEMA (10 mmol, 1.3 g) except for LBBn$_7$(OF$_3$iP)$_2$ and LBBn$_7$(OF$_6$iP)$_2$ synthesis which used PEGMA with a molecular weight of 360 g.mol^{-1} (10 mmol, 3.6 g). The solutions were stirred with argon flow and subsequently cooled in an acetone-liquid nitrogen bath, avoiding solidification of the system. 1 eq. of BH$_3$-THF complex solution of 1 M in THF (10 mmol, 10 ml) was carefully added "dropwise." At the same time, H$_2$ was expelled from the system with nitrogen flow. Then, the reaction mixtures were slowly warmed to RT and stirred for 30 min more. Before adding the subsequent reagents, the systems were cooled in an acetone-liquid nitrogen bath. Afterward, the systems were heated to RT for 1 hour to ensure that H$_2$ releases were complete. 2 eq. of alcohols according to the desired monomer were added dropwise such as HFiP (20 mmol, 4 ml) for LBBn$_1$(OF$_6$iP)$_2$ and LBBn$_7$(OF$_6$iP)$_2$; TFP (20 mmol, 4 ml) for LBBn$_7$(OF$_3$iP)$_2$; and TEG (20 mmol, 4 ml) for LBBn$_1$(OGly)$_2$. For LBBn$_1$(OGlyOF$_6$iP) and LBBn$_1$(OGlyOF$_3$iP), two different alcohols were added dropwise separately: first, 1 eq. of TEG (10 mmol, 4 ml), and secondly, 1 eq. of HFiP for LBBn$_1$(OGlyOF$_6$iP) and TFP (10 mmol, 4 ml) for LBBn$_1$(OGlyOF$_3$iP). Finally, for each synthesis, 1 eq. of nBuLi 2.5 M in hexane (10 mmol, 4 ml) was added dropwise following the same temperature control protocol. The reaction mixture was stirred at RT for another 2 hours. Finally, the product was precipitated and washed with cold diethyl ether. The monomers obtained were placed in vials and dried in a vacuum line at 40 °C for 24h.

pLBBn$_1$(OMe)$_2$. Yield: 0.9 g (97 %). ^{1}H NMR (400 MHz, D$_2$O): δ (ppm) = 3.75-3.44 (dt, 4H, CO-O-C̲H̲$_2$-C̲H̲$_2$-O-B), 3.24 (s, 6H, B-O-C̲H̲$_3$), 1.72 (s, 3H, CH$_2$-C(C̲H̲$_3$)-CH$_2$), 1.49 (q, 2H, B-C̲H̲$_2$-CH$_2$-), 1.32 (sx, 4H, B-CH$_2$-C̲H̲$_2$-CH$_2$), 1.24 (br, 2H, -(C̲H̲$_2$-C(CH$_3$))-), 0.87 (t, 3H, (CH$_2$)$_3$-C̲H̲$_3$); ^{11}B NMR (400 MHz, D$_2$O): δ (ppm) = 3.8 (s, -CH$_2$-B̲-(OR)$_2$).

pLBBn$_7$(OMe)$_2$. Yield: 0.9 g (89 %). ^{1}H NMR (400 MHz, D2O): δ (ppm) = 3.59 (dt, 28H, CO-O-(C̲H̲$_2$-C̲H̲$_2$)$_7$-O-B), 2.54 (sx, 6H, B-O-C̲H̲$_3$), 1.70 (s, 3H, CH$_2$-C(C̲H̲$_3$)-CH$_2$), 1.47 (q, 2H, B-C̲H̲$_2$-CH$_2$-), 1.30 (q, 2H, B-CH$_2$-C̲H̲$_2$-CH$_2$-), 1.20 (br, 2H, -(C̲H̲$_2$-C(CH$_3$))-), 1.01 (m, 2H, B-(CH$_2$)$_2$-C̲H̲$_2$-CH$_3$), 0.83 (q, 3H, (CH$_2$)$_2$-C̲H̲$_3$); ^{11}B NMR (400 MHz, D$_2$O): δ (ppm) = 2.5 (s, -CH$_2$-B̲-(OR)$_2$).

pLBBn$_9$(OMe)$_2$. Yield: 1.9 g (63%). 1H NMR (400 MHz, D2O): δ (ppm) = 3.70-3.60 (dt, CO-O-(C̲H̲$_2$-C̲H̲$_2$)$_9$-O-B), 2.54 (s, 6H, B-O-C̲H̲$_3$), 1.71 (s, 3H, CH$_2$-C(C̲H̲$_3$)-CH$_2$), 1.48 (q, 2H, B-C̲H̲$_2$-CH$_2$-), 1.30 (q, 2H, B-CH$_2$-C̲H̲$_2$-CH$_2$-), 1.22 (br, 2H, -(C̲H̲$_2$-C(CH$_3$))-), 1.01 (q, 2H, B-(CH$_2$)$_2$-C̲H̲$_2$-CH$_3$), 0.82 (t, 3H, (CH$_2$)$_3$-C̲H̲$_3$); ^{11}B NMR (400 MHz, D$_2$O): δ (ppm) = 2.4 (s, -CH$_2$-B̲-(OR)$_2$).

pLBBn$_1$(OEt)$_2$. Yield: 1.25 g (91 %). ^{1}H NMR (400 MHz, D$_2$O): δ (ppm) = 3.63-3.56 (dt, 4H, CO-O-C̲H̲$_2$-C̲H̲$_2$-O-B), 3.31 (c, 4H, B-O-C̲H̲$_2$), 1.71 (s, 3H, CH$_2$-C(C̲H̲$_3$)-CH$_2$), 1.48 (q, 2H, B-C̲H̲$_2$-CH$_2$-), 1.29 (sx, 2H, B-CH$_2$-C̲H̲$_2$-CH$_2$), 1.21 (br, 2H, -(C̲H̲$_2$-C(CH$_3$))-), 1.14 (t, 6H, B-O-CH$_2$-C̲H̲$_3$), 0.86 (q, 4H, B-(CH$_2$)$_3$-C̲H̲$_3$); ^{11}B NMR (400 MHz, D$_2$O): δ (ppm) = 2.8 (s, -CH$_2$-B̲-(OR)$_2$).

Special issue: Celebrating 50 years of Chemistry at the Universidad Autónoma Metropolitana. Part 1

pLBBn₇(OEt)₂. Yield: 4.1 g (7 7%). ¹H NMR (400 MHz, D₂O): δ (ppm) = 3.61-3.58 (dt, 28H, CO-O-(CH₂-CH₂)₇-O-B), 2.81 (q, 4H, B-O-CH₂), 1.69 (s, 3H, CH₂-C(CH₃)-CH₂), 1.47 (q, 2H, B-CH₂-CH₂-), 1.29 (q, 2H, B-CH₂-CH₂-CH₂-), 1.19 (br, 2H, -(CH₂-C(CH₃))-), 1.13 (t, 6H, B-O-CH₂-CH₃), 1.01 (m, 2H, B-(CH₂)₂-CH₂-CH₃), 0.85 (q, 6H, (CH₂)₃-CH₃); ¹¹B NMR (400 MHz, D₂O): δ (ppm) = 2.3 (s, -CH₂-B-(OR)₂).

pLBBn₁(OiP)₂. Yield: 1.08 g (87 %). ¹H NMR (400 MHz, D₂O): δ (ppm) = 3.98 (m, 2H, B-O-CH(CH₃)₂), 3.67-3.56 (dt, 4H, CO-O-CH₂-CH₂-O-B), 1.71 (s, 3H, CH₂-C(CH₃)-CH₂), 1.49 (q, 2H, B-CH₂-CH₂-), 1.30 (sx, 3H, B-CH₂-CH₂-CH₂), 1.21 (br, 2H, -(CH₂-C(CH₃))-), 1.15 (d, 12H, B-O-CH(CH₃)₂), 1.01 (d, 2H, B-(CH₂)₂-CH₂-CH₃), 0.86 (q, 4H, B-(CH₂)₃-CH₃); ¹¹B NMR (400 MHz, D₂O): δ (ppm) = 2.8 (s, -CH₂-B-(OR)₂).

pLBBn₇(OiP)₂. Yield: 2.1 g (95 %). ¹H NMR (400 MHz, D₂O): δ (ppm) = 3.98 (m, 2H, B-O-CH(CH₃)₂), 3.63-3.49 (dt, 28H, CO-O-(CH₂-CH₂)₇-O-B), 1.71 (s, 3H, CH₂-C(CH₃)-CH₂), 1.49 (q, 2H, B-CH₂-CH₂-), 1.32 (q, 2H, B-CH₂-CH₂-CH₂-), 1.23 (br, 2H, -(CH₂-C(CH₃))-), 1.14-1.12 (d, 12H, B-O-CH(CH₃)₂), 1.01 (m, 2H, B-(CH₂)₂-CH₂-CH₃), 0.86 (q, 3H, (CH₂)₃-CH₃); ¹¹B NMR (400 MHz, D₂O): δ (ppm) = 3.1 (s, -CH₂-B-(OR)₂).

pLBBn₁(OF₆iP)₂. Yield: 1.32 g (91 %). ¹H NMR (400 MHz, D₂O): δ (ppm) = 4.63 (sp, 2H, B-O-CH(CF₃)₂), 3.63-3.56 (dt, 4H, CO-O-CH₂-CH₂-O-B), 1.71 (s, 3H, CH₂-C(CH₃)-CH₂), 1.49 (q, 2H, B-CH₂-CH₂-), 1.30 (sx, 2H, B-CH₂-CH₂-CH₂-), 1.24 (br, 2H, -(CH₂-C(CH₃))-), 1.11 (c, 2H, B-(CH₂)₂-CH₂-CH₃), 0.86 (q, 3H, B-(CH₂)₃-CH₃); ¹¹B NMR (400 MHz, D₂O): δ (ppm) = 7.8 (s, -CH₂-B-(OR)₂); ¹⁹F NMR (400 MHz, D₂O): δ (ppm) = -75.89 (s, CF₃).

pLBBn₇(OF₆iP)₂. Yield: 6.6 g (9 2%). ¹H NMR (400 MHz, D₂O): δ (ppm) = 4.67 (m, 2H, B-O-CH(CF₃)₂), 3.70-3.55 (dt, 28H, CO-O-(CH₂-CH₂)₇-O-B), 1.71 (s, 3H, CH₂-C(CH₃)-CH₂), 1.48 (q, 2H, B-CH₂-CH₂-), 1.30 (sx, 2H, B-CH₂-CH₂-CH₂-), 1.26 (br, 2H, -(CH₂-C(CH₃))-), 1.12 (m, 2H, B-(CH₂)₂-CH₂-CH₃), 0.86 (q, 3H, (CH₂)₂-CH₃); ¹¹B NMR (400 MHz, D₂O): δ (ppm) = 8.8 (s, -CH₂-B-(OR)₂); ¹⁹F NMR (400 MHz, D₂O): δ (ppm) = -75.89 (s, CF₃).

pLBBn₇(OF₃iP)₂. Yield: 2.7 g (68 %). ¹H NMR (400 MHz, D₂O): δ (ppm) = 4.51-4.19 (m, 2H, B-O-CH(CF₃)(CH₃)), 3.70-3.55 (dt, 28H, CO-O-(CH₂-CH₂)₇-O-B), 1.71 (s, 3H, CH₂-C(CH₃)-CH₂), 1.49 (q, 2H, B-CH₂-CH₂-), 1.30 (sx, 2H, B-CH₂-CH₂-CH₂-), 1.26 (br, 2H, -(CH₂-C(CH₃))-), 1.12 (m, 2H, B-(CH₂)₂-CH₂-CH₃), 1.02 (d, 6H, B-O-CH(CF₃)(CH₃)), 0.86 (q, 3H, (CH₂)₃-CH₃); ¹¹B NMR (400 MHz, D₂O): δ (ppm) = 4.3 (s, -CH₂-B-(OR)₂); ¹⁹F NMR (400 MHz, D₂O): δ (ppm) = -75.98 (s, CF₃).

pLBBn₁(OGly)₂. Yield: 3.54 g (68 %). ¹H NMR (400 MHz, D₂O): δ (ppm) = 3.61-3.53 (m, 28H, O-CH₂-CH₂-O), 3.07 (s, 6H, CO-CH₃), 1.65 (s, 3H, CH₂-C(CH₃)-CH₂), 1.43 (m, 6H, B-CH₂-CH₂-), 1.25 (m, 6H, B-CH₂-CH₂-CH₂-), 1.16 (br, 2H, -(CH₂-C(CH₃))-), 1.06 (m, 2H, B-(CH₂)₂-CH₂-CH₃), 0.81 (m, 9H, B-(CH₂)₃-CH₃); ¹¹B NMR (400 MHz, D₂O): δ (ppm) = 3.6 (s, -CH₂-B-(OR)₂).

pLBBn₁(OGlyOF₆iP). Yield: 2.16 g (91 %). ¹H NMR (400 MHz, D₂O): δ (ppm) = 4.47 (sp, 1H, B-O-CH(CF₃)₂), 3.62-3.46 (m, 16H, O-CH₂-CH₂-O), 3.40 (s, 3H, -O-CH₃), 1.62 (s, 3H, CH₂-C(CH₃)), 1.41 (m, B-CH₂-CH₂-), 1.24 (m, B-CH₂-CH₂-CH₂-), 1.07 (m, B-(CH₂)₂-CH₂-CH₃), 1.02 (br, -(CH₂-C(CH₃))-), 0.79 (m, B-(CH₂)₃-CH₃); ¹¹B NMR (400 MHz, D₂O): δ (ppm) = 5.9 (s, -CH₂-B-(OR)₂); ¹⁹F NMR (400 MHz, D₂O): δ (ppm) = -78.2 (s, CF₃).

pLBBn₁(OGlyOF₃iP). Yield: 2.97 g (78 %). ¹H NMR (400 MHz, D₂O): δ (ppm) = 4.51 (sp, 1H, B-O-CH(CF₃)(CH₃)), 3.54-3.63 (m, 28H, O-(CH₂-CH₂)₇-O), 3.49 (s, 3H, -O-CH₃), 1.71 (s, 3H, CH₂-C(CH₃)), 1.49 (m, B-CH₂-CH₂-), 1.30 (m, B-CH₂-CH₂-CH₂-), 1.15 (d, 12H, B-O-CH(CF₃)(CH₃)), 1.10 (m, B-(CH₂)₂-CH₂-CH₃), 1.01 (br, -(CH₂-C(CH₃))-), 0.86 (m, B-(CH₂)₃-CH₃); ¹¹B NMR (400 MHz, D₂O): δ (ppm) = 4.3 (s, -CH₂-B-(OR)₂); ¹⁹F NMR (400 MHz, D₂O): δ (ppm) = -78.2 (s, CF₃).

Special issue: Celebrating 50 years of Chemistry at the Universidad Autónoma Metropolitana. Part 1

The general procedure of polymerization

The synthesized boron-based monomers were used to obtain a series of SLICPEs using the random radical polymerization method. The following example describes the procedure used for the synthesis of the linear polymer pLBBn$_1$(OMe)$_2$: LBBn$_1$(OMe)$_2$ monomer (0.95 g), AIBN (0.0040 g, 3 wt%), and methanol (0.40 ml) were gently mixed in a Schlenk tube at RT. To remove as much oxygen as possible, the system was bubbled for 3 min with a flow of argon and an additional 30 min after the reagents were added. The reaction flask was immersed in a hot oil bath at 60 °C and left for 6h. After the reaction, the polymers were dried on a rotary evaporator, thoroughly dried at 60 °C under vacuum for 24 h, and stored in the glove box. The monomers *LBBn$_1$(OR)$_2$*, *LBBn$_7$(OR)$_2$*, and *LBBn$_9$(OR)$_2$* were used for obtaining pLBBn$_1$(OR)$_2$, pLBBn$_7$(OR)$_2$, and pLBBn$_9$(OR)$_2$ SLICPEs following the same polymerization method described above.

The obtained polymers pLBBn$_1$(OMe)$_2$, pLBBn$_1$(OEt)$_2$, pLBBn$_1$(OiP)$_2$, and pLBBn$_1$(OF$_6$iP)$_2$ were white solid; pLBBn$_7$(OMe)$_2$, pLBBn$_7$(OEt)$_2$, pLBBn$_7$(OiP)$_2$, pLBBn$_9$(OMe)$_2$, pLBBn$_7$(OF$_3$iP)$_2$, pLBBn$_1$(OGly)$_2$, pLBBn$_1$(OGlyOF$_3$iP) were gels; and pLBBn$_7$(OF$_6$iP)$_2$, pLBBn$_1$(OGlyOF$_6$iP) were viscous liquids.

Preparation of SLICPEs

The SLICPEs made with the white solid polymers such as pLBBn$_1$(OMe)$_2$, pLBBn$_1$(OEt)$_2$, pLBBn$_1$(OiP)$_2$, and pLBBn$_1$(OF$_6$iP)$_2$ were prepared by dissolution, drop-casting, and evaporation. A solution of 10 wt.% of polymer in MeOH was mixed, and 200 µL was drop-casted onto an 11 mm diameter silicone mold. First, the SLICPEs were dried at RT under nitrogen flow for 6h and then under vacuum in a BUCHI glass oven at 60 °C for 2h. The SLICPEs made with the gel polymers such as pLBBn$_7$(OMe)$_2$, pLBBn$_7$(OEt)$_2$, pLBBn$_7$(OiP)$_2$, pLBBn$_9$(OMe)$_2$, pLBBn$_7$(OF$_3$iP)$_2$, pLBBn$_1$(OGly)$_2$, and pLBBn$_1$(OGlyOF$_3$iP) were prepared with a hot press at 60 °C under 10 bars for 5 min. The thickness of the obtained membranes for the gel polymers was around 70 µm. The viscous liquid polymers such as pLBBn$_7$(OF$_6$iP)$_2$ and pLBBn$_1$(OGlyOF$_6$iP) were used as is, without any particular physical preparation for tests.

The tests with gel SLICPEs in contact with lithium metal, the polymers were used in an Ar–filled glove box. In the first step, the polymers were placed inside sealed airtight pockets inside the glove box to be pressed at 60 °C under 10 bars for 5 min, avoiding moisture environment contact. In the second step, the lithium metal was placed on the made SLICPE membrane and closed together inside a sealed airtight pocket to be pressed in the same condition that it had previously been.

Results and discussion

Synthesis of lithium borate monomers and their single lithium-ion conducting polymers

The methacrylic borate SLICPEs studied in this work were synthesized following the three steps shown in Fig. 1(**a**). Different ethoxy methacrylate monomers were chosen as reactants: 2-hydroxyethyl methacrylate (HEMA) to have one ethoxy repeating unit as linker (n$_1$), and two poly(ethylene glycol) methacrylates to have seven and nine ethoxy repeating units (n$_7$, and n$_9$ respectively). The first step of the synthesis involves the covalent bonding of the ethoxy methacrylate group to the boron atom by a -C-O-B- bond. This step is carried out using two different methods: A and B methods, which are detailed in Fig. 1(**b**) and Fig. 1(**c**). Method A allows the synthesis of *BMn(OR)$_2$* in one step by using Tri-R borates as reagents where the R substituents of interest are already bonded to the boron. Method A is used to synthesize the seven SLICPEs with R as aliphatic substituents (methyl, ethyl, and isopropyl): pLBBn$_1$(OMe)$_2$, pLBBn$_1$(OEt)$_2$, pLBBn$_1$(OiP)$_2$, pLBBn$_7$(OMe)$_2$, pLBBn$_7$(OEt)$_2$, pLBBn$_7$(OiP)$_2$, pLBBn$_9$(OMe)$_2$. Method B splits the one-step method A into two steps; it is used for reagents where the R substituents of interest are not bonded to the boron. The steps include adding Borane to obtain the bond with the boron atom in the form -C-O-BH$_2$, then adding the alcohol R-OH to get the two desired -O-R substituents in *BMn(OR)$_2$*.
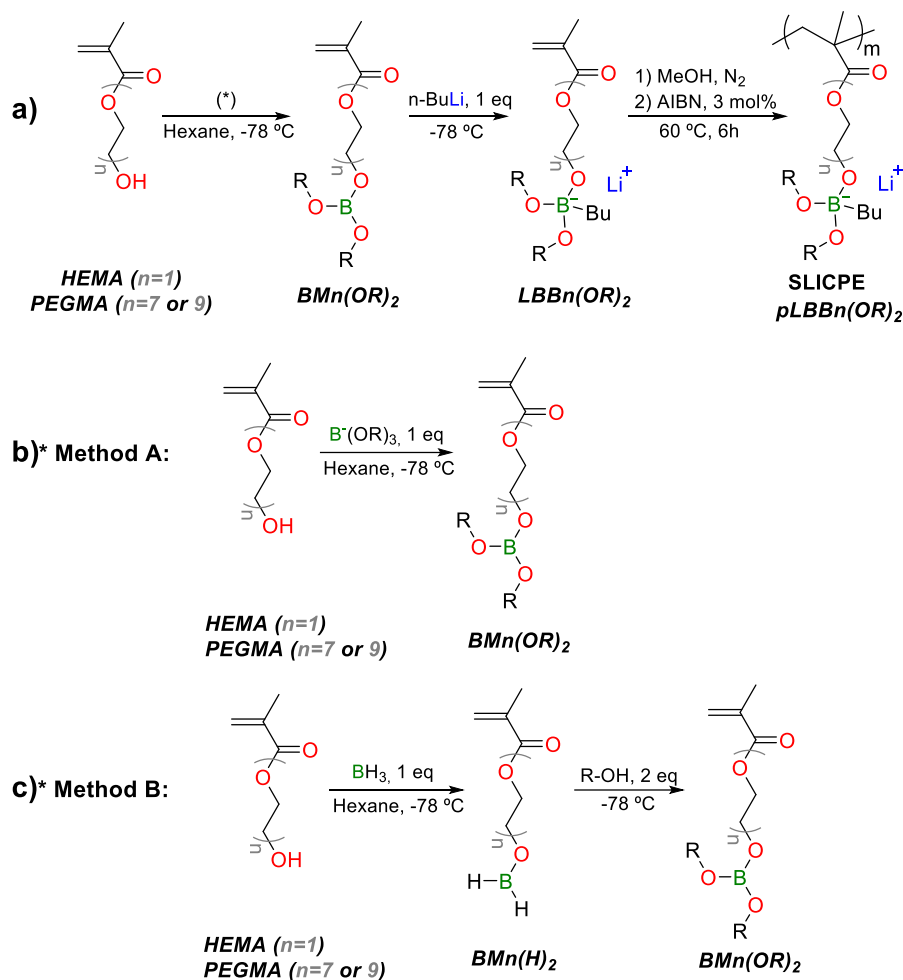
Fig. 1. (a) Synthetic routes for the general preparation of *pLBBn(OR)₂*, and the two synthetic routes to prepare monomers *BMn(OR)₂* following the **(b)** method A, and **(c)** method B.

In the second stage (Fig. 1(**a**)), nBuLi is added to the boron atom to give rise to the formation of the boron-lithium salts of the form *LBBn(OR)₂*, generating a covalent bond (-C-B-). Finally, the different monomers were polymerized in the last stage using a conventional free radical polymerization method, adding AIBN as an initiator. After the reaction, the polymers were purified, dried, and stored in the glove box.

All synthesized polymers are summarized in Table S1 with their corresponding name. Polymers, including three different linkers, were designed with one ethoxy unit, seven ethoxy units, or nine ethoxy units between the methacrylic polymer chain and the borate anion. They are classified into four categories of lithium borate polymers created according to the chemical characteristics of the substituents such as aliphatic, fluorinated, self-solvating, and the last group includes a fluorinated substituent and an ethylene glycol substituent, as shown in Fig. 2.[34,35]
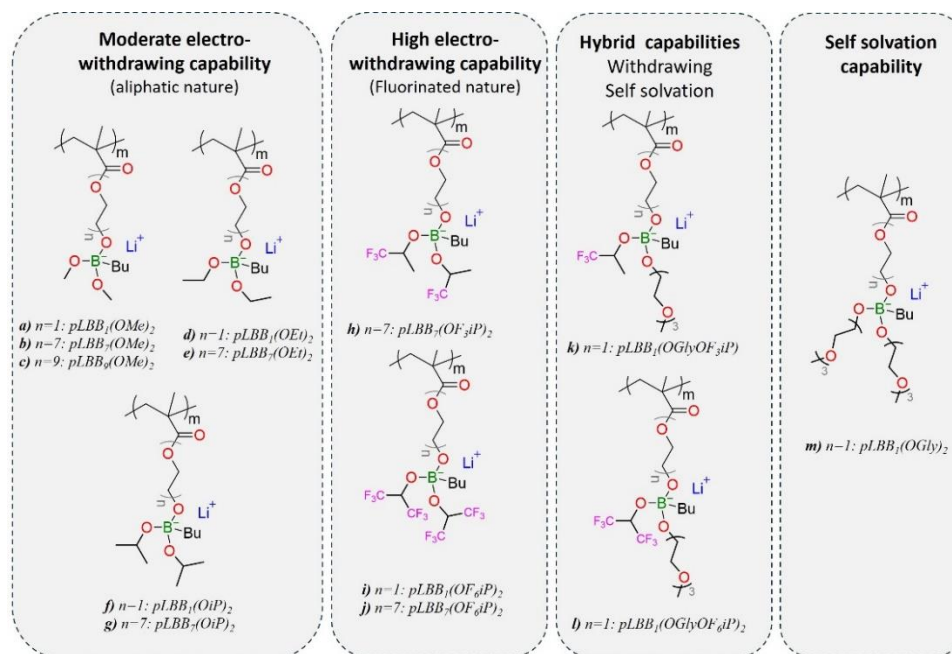
565

Special issue: Celebrating 50 years of Chemistry at the Universidad Autónoma Metropolitana. Part 1

Fig. 2. The chemical structure of synthesized lithium borate SLICPEs.

Structure and thermal characterizations of lithium borate SLIPCEs

NMR and FTIR characterized each monomer and polymer to confirm their chemical structures. For example, Fig. S1 and Fig. 3(a) show the ^{1}H NMR and FTIR spectra with peak assignment for the monomer LBBn$_7$(OMe)$_2$ in blue and polymer pLBBn$_7$(OMe)$_2$ in red. All monomers and polymers present similar signals in ^{1}H NMR spectra (Fig. S1), such as the butyl group bonded to the boron atom in the region of 0.5 to 1.8 ppm, the methyl and polyethylene oxide of the methacrylate group around 1.7 and 3.5-3.7 ppm respectively. Depending on the substituents bound to the boron, the NMR signal is different, and in the context of our example, it is the methyl group found at 2.5 and 2.8 ppm. The typical markers of methyl methacrylate monomers are the vinylic protons between 5.2 and 6.2 ppm corresponding to the methylene group, which are absent for the polymers, confirming the total polymerization in addition to the methyl signal around 1.2 ppm. The FTIR spectra (Fig. 3(**a**)) show similar peaks for monomers and polymers corresponding to the alkane groups between 2800 and 3000 cm^{-1} and for carbonyl groups at 1710 cm^{-1}. Besides, the peak corresponding to the alkene groups at 1635 cm^{-1} is present for the monomers and absent for the polymers, which once again confirms the full extent of the polymerization.

Fig. 3(**b**) shows the ^{1}H NMR spectra for pLBBn$_7$(OiP)$_2$, pLBBn$_7$(OF$_3$iP)$_2$, and pLBBn$_7$(OF$_6$iP)$_2$ polymers. In general, the assignment of peaks in the ^{1}H NMR spectra shows a septet associated with the unprotected carbon-alpha proton of the (1,1,1,3,3,3-hexafluoropropan-2-yl)oxy with a chemical shift at 4.7 ppm for pLBBn$_7$(OF$_6$iP)$_2$. The septet signal shows a decrease in intensity and a shift to the high field (4.2 ppm) due to the effect of the substitution of three fluorine atoms by hydrogens as a substituent in the SLICPE pLBBn$_7$(OF$_3$iP). This behaviour is even more pronounced for the SLICPE pLBBn$_7$(OiP)$_2$, in which hydrogens substitute all fluorine atoms, and the septet is shifted to 4.0 ppm.

In addition to ^{1}H NMR analysis, ^{11}B and ^{19}F NMR spectra were studied to complement the analysis of the chemical structure of monomers and polymers and to elucidate the effect of the different electron-withdrawing groups on the electron density of the borate group. Due to the similar molecular structures of SLICPEs pLBBn$_7$(OiP)$_2$, pLBBn$_1$(OGly)$_2$, pLBBn$_1$(OGlyOF$_3$iP), pLBBn$_7$(OF$_3$iP)$_2$, pLBBn$_1$(OGlyOF$_6$iP), and pLBBn$_7$(OF$_6$iP)$_2$ SLICPEs these were selected for comparison and analysis of the degree of deprotection and electron density of the central boron atom, these were selected for comparison and analysis of the degree of deprotection and electron density of the central boron atom by ^{11}B NMR (Fig. S2). This is related to the chemical shifts of the signals towards the low field,

566

Special issue: Celebrating 50 years of Chemistry at the Universidad Autónoma Metropolitana. Part 1

indicating less interaction with other nuclei, and is related to the increased mobility of the lithium ions through the shift of single ^{11}B NMR signal associated with the tetra-coordinated boron atoms.[36-38]

The chemical shift of the $pLBBn_7(OiP)_2$ signal is between 2.3 and 3.8 ppm for the other aliphatic polymers (Fig. S2.i). The signals are located in the high fields due to the moderate electron-withdrawing groups of aliphatic substituents, which do not influence the electron density of the boron atom. In the same way, $pLBBn_1(OGly)_2$ has a signal with a chemical shift of 3.6 ppm (Fig. S2.ii). Regarding the signals of polymers $pLBBn_1(OGlyOF_3iP)$, $pLBBn_7(OF_3iP)_2$, $pLBBn_1(OGlyOF_6iP)$, and $pLBBn_7(OF_6iP)_2$, they have chemical shifts of 4.3, 4.3, 5.9, and 8.8 (Fig. S2-iii-vi). The chemical shifts move towards lower fields than the aliphatic polymers, implying a higher degree of deprotection and decreased electron density on the boron atom. This effect is related to the fluorinated groups, which increase the electro-withdrawing capability. We can notice the correlations between the evolution of chemical shifts and the increase of fluorine atoms for $pLBBn_7(OiP)_2 <$ $pLBBn_7(OF_3iP)_2 < pLBBn_7(OF_6iP)_2$ and for $pLBBn_1(OGly)_2 < pLBBn_1(OGlyOF_3iP) < pLBBn_1(OGlyOF_6iP)$.
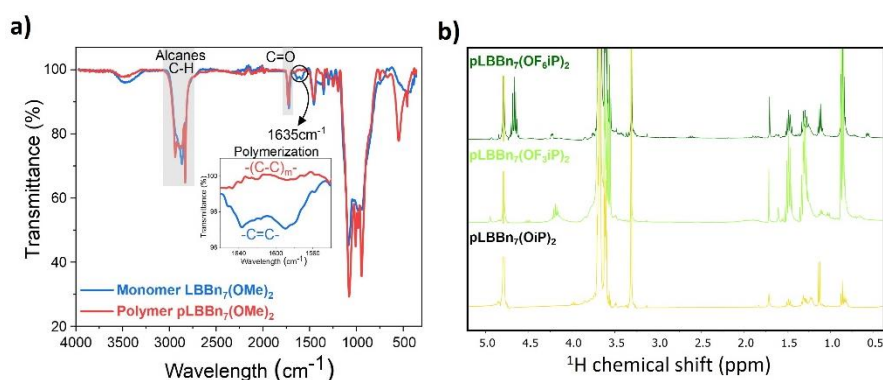
Fig. 3. (a) FTIR spectra for monomer $LBBn_7(OMe)_2$ and polymer $pLBBn_7(OMe)_2$; and **(b)** ^1H NMR spectra for $pLBBn_7(OiP)_2$, $pLBBn_7(OF_3iP)_2$, and $pLBBn_7(OF_6iP)_2$.

Table S2 reports the Tg values determined by the DSC technique. All the polymers reported are amorphous, and their Tg values are below -40 °C. In the first instance, the Tg values obtained for the $pLBBn_1(OR)_2$ type SLICPEs are compared. The lowest value of tg = -73 °C is presented for the $pLBBn_1(OGly)_2$ SLICPEs and is associated with the mobility of the pendant ethoxy chains to the borate group, which confers a high intrinsic ability to self-solubilize due to the easy interaction of the ions with the ethoxy groups. The decrease of free ethoxy groups in SLICPE $pLBBn_1(OMe)_2$ decreases the mobility of the chains which is reflected in the increase of the value of Tg = -65 °C. The SLICPE $pLBBn_1(OGlyOF_6iP)_2$ with a value of Tg = -60 °C goes out of the trend, which is associated with a strong interaction between fluorinated groups and lithium ions that decreases the mobility of the principal and pendant polymer chains of SLICPE.

Now, consider the Tg values of $pLBBn_7(OR)_2$ SLICPEs type. Here, the mode of the ethoxy chain linking the main chain of the polymers with borate groups is a crucial factor. The decrease of Li^+ in SLICPEs, due to the increase of the O/Li^+ ratio, is not the primary determinant in the system. The size and electron-withdrawing ability of the substituent groups on the borate groups play a significant role in affecting the chain mobility of SLICPEs. This refers to the Tg values of -55, -50, and -40 °C obtained for SLICPEs $pLBBn_7(OMe)_2$, $pLBBn_7(OEt)_2$, and $pLBBn_7(OF_6iP)_2$, respectively.

Ionic conductivity of borate SLIPCEs

The ionic conductivity of each new borate SLICPE was measured, and the results are discussed using three comparison axes. Firstly, we compare the three SLICPEs *pLBBn(OMe)₂*, composed with methyl-oxy substituents in the borate pendant groups and differentiated with an increasing number of ethoxy units in the linker such as n_1, n_7, or n_9. Secondly, optimized SLICPEs with ethoxy linker fixed at n_7 and some different aliphatic and fluorinated oxy substituents in the borate pendant groups are discussed. Thirdly, the influence of the fluorine number on ionic conductivity is examined by comparing SLICPE.

Special issue: Celebrating 50 years of Chemistry at the Universidad Autónoma Metropolitana. Part 1

Effect of size of the ethoxy linker between the methacrylic polymer and borate group (n_1, n_7, and n_9)

First, we investigated the effect of increasing the number of ethoxy units (n_1, n_7, and n_9) on the linker between the methacrylic polymer backbone and the borate group on the ionic conduction properties. The compared SLICPEs must be composed of similar final substituents -$(OR)_2$, chosen by methyl-oxy substituents to have a single variable to assess the effect of ethoxy repeat unit length properly. The chemical structures and pictures of the concerning *pLBBn(OMe)$_2$*, which are pLBBn$_1$(OMe)$_2$, pLBBn$_7$(OMe)$_2$, and pLBBn$_9$(OMe)$_2$, are shown in Fig. 4**(a)**. Their ionic conductivity results are shown in Fig. 4**(b)**. Exclusively in this part for simplicity, pLBBn$_1$(OMe)$_2$, pLBBn$_7$(OMe)$_2$, and pLBBn$_9$(OMe)$_2$ will be referred to n_1, n_7, and n_9. The increase in the size of the linker showed an effect on the physical appearance of the polymers. This effect was well observed for *pLBBn(OMe)$_2$,* as shown in Fig. 4**(a)**, which is a powder for n_1 and viscous solids for n_7 and n_9.[39,40]
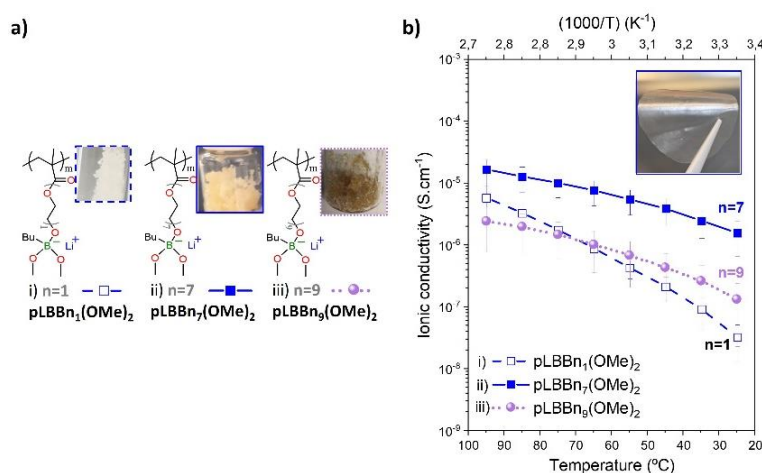

Fig. 4. Comparison of select SLICPEs *pLBBn(OMe)$_2$* type: **(a)** Chemical structures and pictures and b(of SLICPEs and **(b)** the temperature dependence of the ionic conductivity for SLICPEs. i) *pLBBn$_1$(OMe)$_2$*, ii) *pLBBn$_7$(OMe)$_2$*, and iii) *pLBBn$_9$(OMe)$_2$*.

As shown in Fig. 4**(b)**, the highest ionic conductivity is measured for the SLICPE with intermediate ethoxy length (n_7) for all temperatures between 25 and 95 °C. Indeed, the ionic conductivity values for n_7 were 1.58×10^{-6} and 7.64×10^{-6} S cm^{-1} at 25 and 60 °C respectively, whereas the values were less than 10^{-6} S.cm^{-1} for n_1 and n_9 (3.29×10^{-8}, and 8.86×10^{-7} S cm^{-1} for n_1 and 1.33×10^{-7}, and 1.02×10^{-6} S cm^{-1} for n_9 at 25, and 60 °C, respectively). The increase in ionic conductivity with the increase in the ethoxy repeat unit from 1 to 7 can be explained by the O/Li$^+$ ratio, which increases from 5 to 11. In other words, the contribution of ethoxy groups helps the self-solvating ability of borate groups, providing better ionic transport pathways for n_7 than for n_1. However, when the number of ethoxy repeat units was increased beyond 7, for example, at n9, the measured ionic conductivity was lower, although the O/Li$^+$ ratio increased to 13. In conclusion, the self-solvation capability is improved but also limited with the Li$^+$ concentration. The optimized O/Li$^+$ ratio seems to be around 11, corresponding to a polymer with an intermediate ethoxy linker (seven units) for the aliphatic substituents.

Table 1. The activation energy for *pLBBn(OMe)$_2$* SLICPEs with n_1, n_7, and n_9.

Name	Ea (eV)
pLBB$_1$(OMe)$_2$	0.302
pLBB$_7$(OMe)$_2$	0.136
pLBB$_9$(OMe)$_2$	0.176

Special issue: Celebrating 50 years of Chemistry at the Universidad Autónoma Metropolitana. Part 1

Moreover, the activation energies (E_a) were calculated using the Arrhenius equation (2), and the values for the three *pLBBn(OMe)₂* SLICPEs are presented in Table 1. The E_a values provide information on the strength of the coulombic interactions and can be related to the temperature dependence of the ionic conductivity. The E_a value for n₇ and n₉ (0.136 and 0.176 eV respectively) are close, the curves have parallel behaviors to each other in the function of the temperature, whereas E_a for n₁ (0.302 eV) is much larger and shows a very temperature-dependent behavior. The ionic conductivity trend was reversed between n_1 and n_9 above 70 °C. n_1 shows a greater temperature dependence with ionic conductivity values of 3.29×10^{-8} and 5.81×10^{-6} S.cm⁻¹ at 25 °C and 90 °C respectively, whereas the ionic conductivity was more constant for n_9 with values of 1.34×10^{-7} and 2.44×10^{-6} S.cm⁻¹ at 25 and 90 °C respectively. Besides being explained by the values of E_a, this behaviour is due to the generation of spaces and conduction pathways due to the movement of substituent groups compared to the proportion of the polymer. The ionic transport is through hopping between the borate anionic centers for n_1, whereas it is preferentially promoted by the movement of the ethoxy chains for n_7 and n_9.

Effect of the different borate substituents with the ethoxy linker of n₇

Based on the previous study, four SLICPEs with the best ethoxy linker showing 7 units (*pLBBn₇(OR)₂*) and different aliphatic or fluorinated substituents were compared in Fig. 5. The chemical structures and pictures of the concerning *pLBBn₇(OR)₂* are shown in Fig. 5(**a**), and their ionic conductivity results in Fig. 5(**b**). pLBBn₇(OF₆iP)₂ is a viscous liquid polymer as shown the picture in Fig. 5(**a-i**). The three other polymers are malleable materials forming excellent transparent films (pictures in Fig. 5(**a-ii-iv**)).
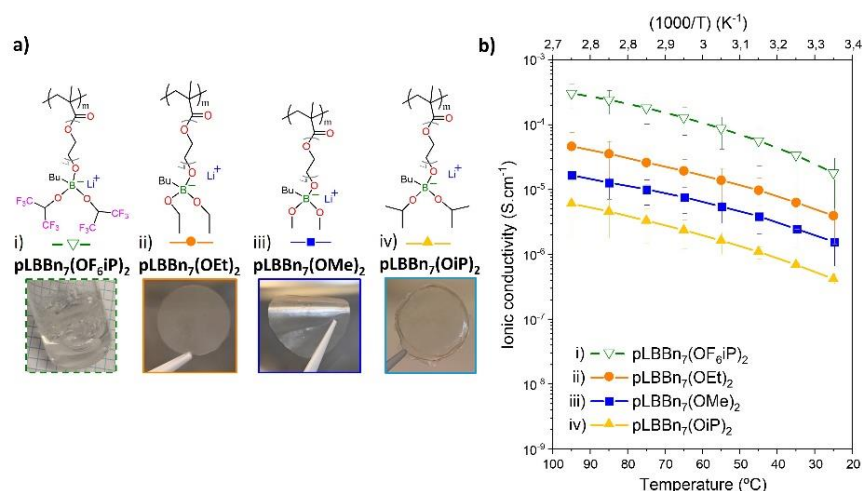

Fig. 5. (**a**) Chemical structures and pictures of n₇ SLICPEs i) pLBBn₇(OF₆iP)₂, ii) pLBBn₇(OEt)₂, iii) pLBBn₇(OMe)₂, and iv) pLBBn₇(OiP)₂; and (**b**) temperature dependence of the ionic conductivity for n₇ SLICPEs.

As a trend, the ionic conductivity curves (Fig. 5(**b**)) are higher for the four SLICPEs n_7, with values of 1.58×10^{-6}, 3.95×10^{-6}, 4.18×10^{-7}, 1.80×10^{-5} S.cm⁻¹ at 25 °C for pLBBn₇(OMe)₂, pLBBn₇(OEt)₂, pLBBn₇(OiP)₂, pLBBn₇(OF₆iP)₂; compared to their n_1 homolog, with values of 3.29×10^{-8}, 4.42×10^{-9}, 7.78×10^{-9}, 2.35×10^{-7} S.cm⁻¹ at 25 °C for pLBBn₁(OMe)₂, pLBBn₁(OEt)₂, pLBBn₁(OiP)₂, pLBBn₁(OF₆iP)₂ respectively (Fig. S3). Moreover, n_7 SLICPEs depend less on temperature than their n_1 counterpart, and n_7 aliphatic SLICPEs follow a similar trend between them with increasing order pLBBn₇(OiP)₂ < pLBBn₇(OMe)₂ < pLBBn₇(OEt)₂.

The ionic conductivity is greatly improved with the fluorinated substituents for pLBBn₇(OF₆iP)₂. This can be explained by the decrease in the electron density of the boron atom, as shown in the ¹¹B NMR study previously. The boron atom is highly deprotected for pLBBn₇(OF₆iP)₂ compared to the aliphatic ones due to the electronic delocalization effect with the electron-withdrawing fluorinated substituents. The interaction energy between Li⁺ and the borate group is lower for pLBBn₇(OF₆iP)₂ helping the Li-ions mobility. In addition, the viscous liquid texture promotes the mobility of ions compared to materials in the form of films.

569

The ionic conductivity of pLBBn$_7$(OF$_6$iP)$_2$ with values of 1.80×10^{-5}, 1.29×10^{-4}, and 3.05×10^{-4} Scm^{-1} at 25, 60, and 90 °C respectively, follows very closely the ionic conductivity of pLBBn$_1$(OGlyOF$_6$iP) with values of 3.26×10^{-5}, 1.65×10^{-4}, and 3.28×10^{-4} S cm^{-1} at 25, 60 and 90 °C respectively. pLBBn$_7$(OF$_6$iP)$_2$ has an O/Li ratio of 11 mainly due to its intermediate ethoxy linker (n$_7$) and a F/Li ratio of 12 thanks to its two identic pendant groups isopropyl-oxy with six fluorine atoms (-O-CH-(CF$_3$)$_2$). Its chemical structure promotes ionic conductivity with the effects of lithium solvation by oxygen atoms and of the delocalization of the anionic charge of the boron atom with the electro-withdrawing groups. pLBBn$_1$(OGlyOF$_6$iP) comprises a shorter ethoxy linker (n$_1$). Still, its O/Li ratio is 8, which is higher than for the aliphatic n$_1$ SLICPEs (O/Li ratio of 5), and this is due to one of its pendant groups constituted of glycol substituents. The other pendant group is an isopropyl-oxy substituent with six fluorine atoms (-O-CH-(CF$_3$)$_2$), which gives an F/Li ratio of 6. The ^{11}B NMR study shows signals for pLBBn$_7$(OF$_6$iP)$_2$ and pLBBn$_1$(OGlyOF$_6$iP) with chemical shifts of 8.8 and 5.9 ppm, respectively (Fig. S2-v-vi), which are in the lowest fields compared with the other studied polymers. The degree of deprotection of the borate group is higher for pLBBn$_7$(OF$_6$iP)$_2$ than for pLBBn$_1$(OGlyOF$_6$iP), which means the interaction energy between Li and borate group is lower for pLBBn$_7$(OF$_6$iP)$_2$ (Fig. S4). However, contrary to the values of the ratios, the size of the electron-withdrawing group, and the NMR study, the ionic conductivity of pLBBn$_7$(OF$_6$iP)$_2$ is slightly lower than for pLBBn$_1$(OGlyOF$_6$iP). The difference is probably due to the geometry of the polymers. The ethoxy chain on the pendant position on the boron atom for pLBBn$_1$(OGlyOF$_6$iP) gives more availability for the lithium solvation, unlike the position between the boron and polymer backbone. A modeling study could help to understand and validate this hypothesis.

Influence of the fluorine content of the substituents

In this part, the evolution of ionic conductivity is discussed for two comparison cases of SLICPEs with different numbers of fluorine atoms and the same structures. In the first case, pLBBn$_1$(OGlyOF$_3$iP) and pLBBn$_1$(OGlyOF$_6$iP) are compared, their chemical structures and pictures are shown in Fig. 6(**a.i-ii**), and their ionic conductivity results in Fig. 6(**b**). For the second case, pLBBn$_7$(OiP)$_2$, pLBBn$_7$(OF$_3$iP)$_2$, and pLBBn$_7$(OF$_6$iP)$_2$ are shown in Fig. 6(**a.iii-v**), and Fig. 6(**c**).
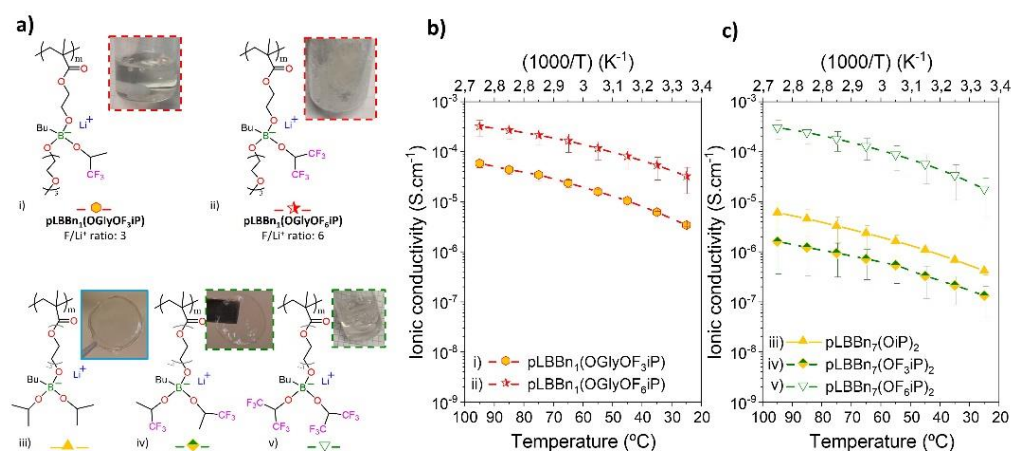
Fig. 6. (a) Chemical structures and pictures of SLICPEs i) pLBBn$_1$(OGlyOF$_3$iP), ii) pLBBn$_1$(OGlyOF$_6$iP), iii) pLBBn$_7$(OiP)$_2$, iv) pLBBn$_7$(OF$_3$iP)$_2$, and v) pLBBn$_7$(OF$_6$iP)$_2$. Temperature dependence of ionic conductivity for **(b)** SLICPEs with 1 ethoxy linker (i-ii), and **c)** SLICPEs with 7 ethoxy linkers (iii-v).

In the first case (Fig. 6(**a.i-ii**) and Fig. 6(**b**)), the SLICPEs pLBBn$_1$(OGlyOF$_3$iP) and pLBBn$_1$(OGlyOF$_6$iP) are compared. Although they are composed of the ethoxy linker of n$_1$, they have an O/Li$^+$ ratio of 8, which is higher than for the aliphatic n$_1$ SLICPEs (O/Li$^+$ ratio of 5) and this is due to the glycol

Special issue: Celebrating 50 years of Chemistry at the Universidad Autónoma Metropolitana. Part 1

substituent on pendant groups. As discussed before, the increase of the O/Li$^+$ ratio helps the lithium-ion solvation, and this can explain why pLBBn$_1$(OGlyOF$_3$iP) and pLBBn$_1$(OGlyOF$_6$iP) have higher ionic conductivity than the aliphatic *pLBBn$_1$(OR)$_2$*. In addition, pLBBn$_1$(OGlyOF$_3$iP) and pLBBn$_1$(OGlyOF$_6$iP) have a similar geometric structure with two pendant groups linked to the boron, which are: one group of triethylene glycol monomethyl ether, and the other group is an isopropyl-oxy geometry with different atoms. The isopropyl-oxy group is composed of six atoms of fluorine (-O-CH-(CF$_3$)$_2$) with a symmetric arrangement for pLBBn$_1$(OGlyOF$_6$iP) while pLBBn$_1$(OGlyOF$_3$iP) has a hybrid composition with three atoms of fluorine and three of hydrogen (-O-CH-(CF$_3$)(CH$_3$)) with an asymmetric arrangement. So, the F/Li$^+$ ratio increases from 3 to 6 for pLBBn$_1$(OGlyOF$_3$iP) and pLBBn$_1$(OGlyOF$_6$iP), respectively. This increase in the F/Li$^+$ ratio slightly impacts the energy density of the borate groups, as it was observed in the ^{11}B NMR study with chemical shifts of 4.3 and 5.9 ppm for pLBBn$_1$(OGlyOF$_3$iP) and pLBBn$_1$(OGlyOF$_6$iP) respectively (Fig. S2-iii and v). The ionic conductivity values also increase, from 3.43×10^{-6} to 3.26×10^{-5} S.cm^{-1} at 25 °C for pLBBn$_1$(OGlyOF$_3$iP), and pLBBn$_1$(OGlyOF$_6$iP) respectively. The ionic conductivity higher for pLBBn$_1$(OGlyOF$_6$iP) can be explained once again by the increase in F/Li$^+$ ratio, which strengthens the electron-withdrawing capability on the pendant groups and decreases the electron density on the borate groups. Thus, the Li$^+$ mobility is promoted by a lower interaction energy between Li$^+$ and borate for pLBBn$_1$(OGlyOF$_6$iP) than for pLBBn$_1$(OGlyOF$_3$iP), as confirmed by the ionic conductivity values.

In the second case (Fig. 6(**a.iii-v**) and Fig. 6(**c**)), the SLICPEs have a similar geometric structure composed of two identic groups of isopropyl-oxy geometry with different atoms with increasing fluorine atoms. The two isopropyl-oxy groups are aliphatic (-O-CH-(CH$_3$)$_2$) for pLBBn$_7$(OiP)$_2$, while the six hydrogens on each isopropyl groups are changed for fluorine atoms (-O-CH-(CF$_3$)$_2$) for pLBBn$_7$(OF$_6$iP)$_2$. pLBBn$_7$(OF$_3$iP)$_2$ has a hybrid composition with two isopropyl-oxy groups composed each of three atoms of fluorine and three of hydrogen (-O-CH-(CF$_3$)(CH$_3$)$_2$) in an asymmetric arrangement. The F/Li$^+$ ratio increased from 0, 6, and 12 for pLBBn$_7$(OiP)$_2$, pLBBn$_7$(OF$_3$iP)$_2$, and pLBBn$_7$(OF$_6$iP)$_2$ respectively; and the ionic conductivity values are 4.18×10^{-7}, 1.34×10^{-7}, and 1.80×10^{-5} S.cm^{-1} at 25 °C respectively. It is worth mentioning that the increasing evolution of the ionic conductivity is pLBBn$_7$(OF$_3$iP)$_2$ < pLBBn$_7$(OiP)$_2$ < pLBBn$_7$(OF$_6$iP). The ionic conductivity behaviour of pLBBn$_7$(OF$_3$iP)$_2$ is the lowest and even lower than pLBBn$_7$(OiP)$_2$. Therefore, in other words, the ionic conductivity does not evolve following the F/Li$^+$ ratio in this case. Although the ^{11}B NMR study had shown an evolution of chemical shifts with the increase of fluorine atoms for pLBBn$_7$(OiP)$_2$, pLBBn$_7$(OF$_3$iP)$_2$, and pLBBn$_7$(OF$_6$iP)$_2$ with chemical shifts of 3.1, 4.3, and 8.8 respectively (Fig. S2.i, iv, and vi), the ionic conductivity trend is different for pLBBn$_7$(OF$_3$iP)$_2$. However, we can observe that the chemical shifts do not evolve continuously, and those of pLBBn$_7$(OF$_3$iP)$_2$ and pLBBn$_7$(OF$_6$iP)$_2$ are very close compared to those of pLBBn$_7$(OiP)$_2$. The asymmetric arrangement of (-O-CH-(CF$_3$)(CH$_3$)) groups in pLBBn$_7$(OF$_3$iP)$_2$ probably plays a complex role in lithium mobility, and this hypothesis could be better explained with a modeling study of molecular orbitals.

Lithium transference number and electrochemical stability of optimized SLICPEs

The single lithium-ion conducting characteristics were evaluated by measuring the lithium transference number (t_{Li^+}) for the n$_1$ and n$_7$ optimized homopolymers, which are pLBBn$_1$(OGly)$_2$, pLBBn$_1$(OGlyOF$_6$iP), pLBBn$_7$(OEt)$_2$, and pLBBn$_7$(OF$_6$iP)$_2$. The t_{Li^+} measurements are shown in Fig. 7. The t_{Li^+} values are **0.92**, **0.93**, **0.88**, and **0.96** for pLBBn$_1$(OGly)$_2$, pLBBn(OGlyOF$_6$iP), pLBBn$_7$(OEt)$_2$, and pLBBn$_7$(OF$_6$iP)$_2$ respectively.

These are high values because they are close to 1, as expected for single-ion polymers. The high ionic conductivity values describe the ionic transport in SPE, which is promoted by the molecular structure of the designed polymers.[34] In highly conductive SLICPEs, ionic transport is determined by the degree of negative charge delocalization in anionic centers, which decreases the interaction energy in the ionic pair.[2,38] Furthermore, generally accepted models for Li$^+$ transport in SPEs involve coupling to the segmental motion of the polymer backbone, and a more flexible backbone is naturally beneficial for conductivity.[4]

The resistance is significantly reduced with viscous liquid homopolymers. Indeed, the electrochemical impedance responses show very high resistances for the two solid SLICPEs with resistance around 75 kΩ for pLBBn$_1$(OGly)$_2$ and higher than 1000 kΩ for pLBBn$_7$(OEt)$_2$ (inset Fig. 7(**a**) and Fig. 7(**c**). While the resistance is improved by a decrease of values less than 3 kΩ for the two viscous liquid SLICPEs pLBBn$_1$(OGlyOF$_6$iP) and pLBBn$_7$(OF$_6$iP)$_2$ (inset Fig. 7(**b**) and Fig. 7(**d**)).
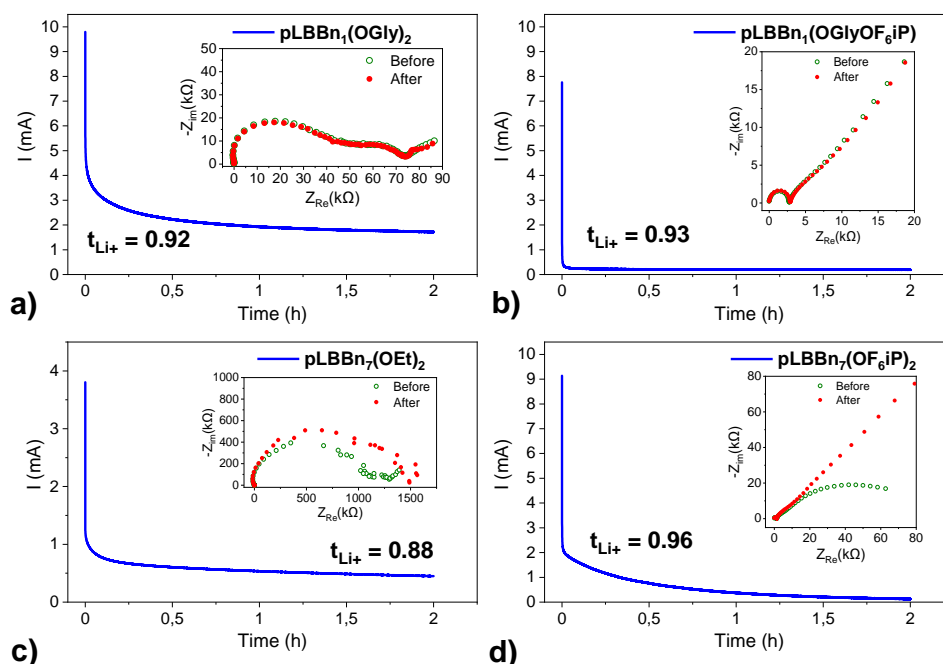
Fig. 7. Lithium transference number (t_{Li+}) evaluation: typical current transient obtained at the polarization of 10 mV for Li|*pLBBn(OR)₂*|Li symmetrical cells at 60 °C (inset: Nyquist plot for the same cell before and after polarization) for the SLICPEs **(a)** pLBBn₁(OGly)₂, **(b)** pLBBn₁(OGlyOF₆iP), **(c)** pLBBn₇(OEt)₂, and **(d)** pLBBn₇(OF₆iP)₂.
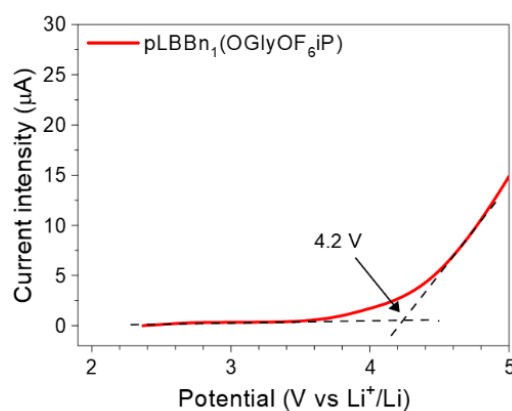
Fig. 8. Linear sweep voltammograms (v = 2 mV.s⁻¹) obtained in the Li| pLBBn₁(OGlyOF₆iP)|stainless steel cell at 60 °C.

To evaluate the electrochemical stability of the homopolymer electrolytes, the cyclic voltammetry of Li|pLBBn(OR)₂|stainless steel cell at 60 °C was studied for pLBBn₁(OGlyOF₆iP). The result in Fig. 8 shows an electrochemical stability close to 4.2 V vs Li⁺/Li, confirming its excellent properties as a solid electrolyte for lithium batteries.

572

Special issue: Celebrating 50 years of Chemistry at the Universidad Autónoma Metropolitana. Part 1

Conclusions

New single-ion lithium conducting polymer electrolytes based on highly delocalized borate groups have been synthesized and characterized. This work shows the effects of the chemical structure on the ionic conductivity values. It highlights the importance of the polymer design in order to achieve the highest ionic conductivity values.

First, the effect study of increasing the ethoxy repeat extender (from n_1, n_7, to n_9) on the ionic conductivity showed the contribution of ethoxy groups helps the self-solvating capability, providing better ionic transport pathways but is also limited. The linker with the highest conductivity is the one with seven ethoxy units n_7 (O/Li$^+$ ratio of 11). As an alternative, the O/Li$^+$ ratio can be increased by playing with the nature of the substituent on the pendant group and not with the ethoxy repeat extender, for example, with glycol groups for pLBBn$_1$(OGly)$_2$ or pLBBn$_1$(OGlyOF$_6$iP).

Then, SLICPEs with optimized ethoxy linkers (n_7 and O/Li$^+$ ratio of 11) and different aliphatic and fluorinated pendant groups showed that the SLICPE with fluorinated pendant groups (pLBBn$_7$(OF$_6$iP)$_2$) achieved the highest ionic conductivity values compared to the aliphatic ones. In fact, increasing the number of fluorine atoms in the substituent groups of SLICPEs improves the electron-withdrawing capacity, which is reflected in the increase of ionic conductivity.

In general conclusion, pLBBn$_1$(OGlyOF$_6$iP) and pLBBn$_7$(OF$_6$iP)$_2$ show, to our knowledge, the highest ionic conductivity reported for a lithium single-conduction homopolymer (1.65×10^{-4} and 1.29×10^{-4} S.cm^{-1} respectively at 60 °C). The single ion-conducting properties were confirmed by its high t_{Li^+}, 0.93 and 0.96 for pLBBn$_1$(OGlyOF$_6$iP), and pLBBn$_7$(OF$_6$iP)$_2$ respectively. The chemical structures of the two optimized SLICEPs are schematized in Fig. 9 with a summary of their properties. Future work will focus on the investigation of the optimized SLIPCEs in lithium batteries.
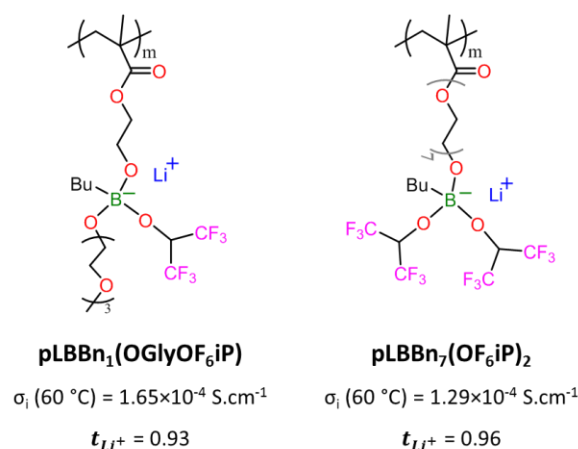

pLBBn$_1$(OGlyOF$_6$iP)
σ_i (60 °C) = 1.65×10^{-4} S.cm^{-1}
t_{Li^+} = 0.93

pLBBn$_7$(OF$_6$iP)$_2$
σ_i (60 °C) = 1.29×10^{-4} S.cm^{-1}
t_{Li^+} = 0.96

Fig. 9. Chemical structures of the two optimized SLICEPs, values of ionic conductivities, and lithium transference number for pLBBn$_1$(OGlyOF$_6$iP) and pLBBn$_7$(OF$_6$iP)$_2$.

Acknowledgments

573

Special issue: Celebrating 50 years of Chemistry at the Universidad Autónoma Metropolitana. Part 1

References

1. Nurul, S.; Mohd, A.; Tajuddin, N. A. *International Journal of Electrochemical Science*. **2021**, *16*, 1–15. DOI: https://doi.org/10.20964/2021.10.53.
2. Zhang, H.; Li, C.; Piszcz, M.; Coya, E.; Rojo, T.; Rodriguez-Martinez, L. M.; Armand, M.; Zhou, Z. *Chem Soc Rev*. **2017**, *3*, 797–815. DOI: https://doi.org/10.1039/c6cs00491a.
3. Zhu, J.; Zhang, Z.; Zhao, S.; Westover, A. S.; Belharouak, I.; Cao, P. F. *Adv Energy Mater*. **2021**, *14*, 1–18. DOI: https://doi.org/10.1002/aenm.202003836.
4. Mindemark, J.; Lacey, M. J.; Bowden, T.; Brandell, D. *Prog. Polym. Sci*. **2018**, *81*, 114–143. DOI: https://doi.org/10.1016/j.progpolymsci.2017.12.004.
5. Xue, Z.; He, D.; Xie, X. *J. Mater. Chem. A Mater*. **2015**, *38*, 19218–19253. DOI: https://doi.org/10.1039/c5ta03471j.
6. Suo, L.; Zheng, F.; Hu, Y. S.; Chen, L. *Chinese Physics B*. **2015**, *1*, 0–4. DOI: https://doi.org/10.1088/1674-1056/25/1/016101.
7. Jiang, Y.; Yan, X.; Ma, Z.; Mei, P.; Xiao, W.; You, Q.; Zhang, Y. *Polymers*. **2018**, *4*, 1–13. DOI: https://doi.org/10.3390/polym10111237.
8. Croce, F.; Appetecchi, G. B.; Persi, L.; Scrosati, B. *Nature*. **1998**, *394*, 456–458. DOI: https://doi.org/10.1038/28818.
9. Guzmán-González, G.; Avila-Paredes, H. J.; Santos-Mendoza, I. *Journal of Solid-State Electrochemistry*. **2023**. DOI: https://doi.org/10.1007/s10008-023-05563-1.
10. Porcarelli, L.; Shaplov, A. S.; Bella, F.; Nair, J. R.; Mecerreyes, D.; Gerbaldi, C. *ACS Energy Lett.* **2016**, *4*, 678–682. DOI: https://doi.org/10.1021/acsenergylett.6b00216.
11. Shan, X.; Zhao, S.; Ma, M.; Pan, Y.; Xiao, Z.; Li, B.; Sokolov, A. P.; Tian, M.; Yang, H.; Cao, P. F. *ACS Appl. Mater Interfaces*. **2022**, *14*, 56110−56119. https://doi.org/10.1021/acsami.2c17547.
12. Guzman Gonzalez, G. *J. Mex. Chem. Soc.* **2023**, *4*, 602–620. DOI: https://doi.org/10.29356/jmcs.v67i4.1959.
13. Porcarelli, L.; Vlasov, P. S.; Ponkratov, D. O.; Lozinskaya, E. I.; Antonov, D. Y.; Nair, J. R.; Gerbaldi, C.; Mecerreyes, D.; Shaplov, A. S. *Eur. Polym. J.* **2018**, *107*, 218–228. DOI: https://doi.org/10.1016/j.eurpolymj.2018.08.014.
14. Zygadła-Monikowska, E.; Florjańczyk, Z.; Ostrowska, J.; Bołtromiuk, P.; Frydrych, J.; Sadurski, W.; Langwald, N. *Electrochim. Acta*. **2011**, *1*, 66–73. DOI: https://doi.org/10.1016/j.electacta.2011.07.120.
15. Guzmán-González, G.; Alvarez-Tirado, M.; Olmedo-Martínez, J. L.; Picchio, M. L.; Casado, N.; Forsyth, M.; Mecerreyes, D. *Adv. Energy Mater*. **2023**, *1*, 2202974. DOI: https://doi.org/10.1002/aenm.202202974.
16. Porcarelli, L.; Shaplov, A. S.; Salsamendi, M.; Nair, J. R.; Vygodskii, Y. S.; Mecerreyes, D.; Gerbaldi, C. *ACS Appl Mater Interfaces*. **2016**, *16*, 10350–10359. DOI: https://doi.org/10.1021/acsami.6b01973.
17. Shaplov, A. S.; Vlasov, P. S.; Armand, M.; Lozinskaya, E. I.; Ponkratov, D. O.; Malyshkina, I. A.; Vidal, F.; Okatova, O. V.; Pavlov, G. M.; Wandrey, C.; Godovikov, I. A.; Vygodskii, Y. S. *Polym Chem*. **2011**, *11*, 2609–2618. DOI: https://doi.org/10.1039/c1py00282a.
18. Meziane, R.; Bonnet, J. P.; Courty, M.; Djellab, K.; Armand, M. *Electrochim Acta*. **2011**, *1*, 14–19. DOI: https://doi.org/10.1016/j.electacta.2011.03.074.
19. Ma, Q.; Zhang, H.; Zhou, C.; Zheng, L.; Cheng, P.; Nie, J.; Feng, W.; Hu, Y. S.; Li, H.; Huang, X.; Chen, L.; Armand, M.; Zhou, Z. *Angewandte Chemie - International Edition*. **2016**, *7*, 2521–2525. DOI: https://doi.org/10.1002/anie.201509299.
20. Zhu, Y. S.; Wang, X. J.; Hou, Y. Y.; Gao, X. W.; Liu, L. L.; Wu, Y. P.; Shimizu, M. *Electrochim Acta*. **2013**, *87*, 113–118. DOI: https://doi.org/10.1016/j.electacta.2012.08.114.
21. Ponkratov, D. O.; Lozinskaya, E. I.; Shaplov, A. S.; Khanin, D. A.; Afanasyev, E. S.; Takazova, R. U.; Vygodskii, Y. S. *Doklady Chemistry*. **2022**, *2*, 29–36. DOI: https://doi.org/10.1134/S0012500822020021.
22. Rolland, J.; Brassinne, J.; Bourgeois, J. P.; Poggi, E.; Vlad, A.; Gohy, J. F. *J Mater Chem. A Mater*. **2014**, *30*, 11839–11846. DOI: https://doi.org/10.1039/c4ta02327g.
23. Rolland, J.; Poggi, E.; Vlad, A.; Gohy, J. F. *Polymer*. **2015**, *68*, 344–352. DOI: https://doi.org/10.1016/j.polymer.2015.04.056.

574

Special issue: Celebrating 50 years of Chemistry at the Universidad Autónoma Metropolitana. Part 1

24. Olmedo-Martínez, J. L.; Porcarelli, L.; Alegría, Á.; Mecerreyes, D.; Müller, A. J. *Macromolecules*. **2020**, *11*, 4442–4453. DOI: https://doi.org/10.1021/acs.macromol.0c00703.
25. Meabe, L.; Goujon, N.; Li, C.; Armand, M.; Forsyth, M.; Mecerreyes, D. *Batter Supercaps.* **2020**, *1*, 68–75. DOI: https://doi.org/10.1002/batt.201900119.
26. Guzmán-González, G.; Vauthier, S.; Alvarez-Tirado, M.; Cotte, S.; Castro, L.; Guéguen, A.; Casado, N.; Mecerreyes, D. *Angewandte Chemie - International Edition*. **2021**, *7*, 1–5. DOI: https://doi.org/10.1002/anie.202114024.
27. Zygadło-Monikowska, E.; Florjańczyk, Z.; Słuzewska, K.; Ostrowska, J.; Langwald, N.; Tomaszewska, A. *J. Power Sources*. **2010**, *18*, 6055–6061. DOI: https://doi.org/10.1016/j.jpowsour.2009.12.097.
28. Meabe, L.; Huynh, T. V.; Lago, N.; Sardon, H.; Li, C.; O'Dell, L. A.; Armand, M.; Forsyth, M.; Mecerreyes, D. *Electrochim Acta.* **2018**, *264*, 367–375. DOI: https://doi.org/10.1016/j.electacta.2018.01.101.
29. Qian, X.; Gu, N.; Cheng, Z.; Yang, X.; Wang, E.; Dong, S. *Journal of Solid-State Electrochemistry*. **2001**, *1*, 8–15. DOI: https://doi.org/10.1007/s100080000190.
30. Menzinger, M.; Wolfgang, R. *Angewandte Chemie International Edition in English*. **1969**, *6*, 438–444. DOI: https://doi.org/10.1002/anie.196904381.
31. Soydan, A. M.; Bozkurt, A. *Ionics*. **2018**, *5*, 1399–1405. DOI: https://doi.org/10.1007/s11581-017-2286-4.
32. Evans, J.; Vincent, C. A.; Bruce, P. G. *Polymer*. **1987**, *13*, 2324–2328. DOI: https://doi.org/10.1016/0032-3861(87)90394-6 .
33. Zugmann, S.; Fleischmann, M.; Amereller, M.; Gschwind, R. M.; Wiemhöfer, H. D.; Gores, H. *J. Electrochim Acta*, **2011**, *11*, 3926–3933. DOI: https://doi.org/10.1016/j.electacta.2011.02.025.
34. Strauss, E.; Menkin, S.; Golodnitsky, D. *Journal of Solid State Electrochemistry*. **2017**, *7*, 1879–1905. DOI: https://doi.org/10.1007/s10008-017-3638-8.
35. Hamaide, T.; Le Deore, C. *Polymer*. **1993**, *5*, 1038–1046. DOI: https://doi.org/10.1016/0032-3861(93)90227-2.
36. Zygadło-Monikowska, E.; Florjańczyk, Z.; Tomaszewska, A.; Pawlicka, M.; Langwald, N.; Kovarsky, R.; Mazor, H.; Golodnitsky, D.; Peled, E. *Electrochim Acta*. **2007**, *4*, 1481–1489. DOI: https://doi.org/10.1016/j.electacta.2007.02.046.
37. Guzmán-González, G.; Ávila-Paredes, H. J.; Rivera, E.; González, I. *ACS Appl Mater Interfaces*. **2018**, *36*, 30247–30256. DOI: https://doi.org/10.1021/acsami.8b02519.
38. Guzmán-González, G.; Ramos-Sánchez, G.; Camacho-Forero, L. E.; González, I. *Journal of Physical Chemistry C*. **2019**, *29*, 17686–17694. DOI: https://doi.org/10.1021/acs.jpcc.9b02945.
39. G. Guzmán, D. Nava, J. Vasquez-Arenas, J. Cardoso, J. A.-Ramirez. *Solid State Ionics*. **2019**, *5*, 55.
40. Nava, D. P.; Guzmán, G.; Vazquez-Arenas, J.; Cardoso, J.; Gomez, B.; Gonzalez, I. *Solid State Ionic.* **2016**, *290*, 98–107. DOI: https://doi.org/10.1016/j.ssi.2016.03.020.

575

Special issue: Celebrating 50 years of Chemistry at the Universidad Autónoma Metropolitana. Part 1